Original

Kumar, R.; Naja, M.; Pfister, G.G.; Barth, M.C.; Brasseur, G.P.:

Source attribution of carbon monoxide in India and surrounding regions during wintertime

In: Journal of Geophysical Research (2013) AGU

DOI: 10.1002/jgrd.50134

JOURNAL OF GEOPHYSICAL RESEARCH: ATMOSPHERES, VOL. 118, 1981–1995, doi:10.1002/jgrd.50134, 2013

Source attribution of carbon monoxide in India and surrounding regions during wintertime

Rajesh Kumar,[1,2,3] Manish Naja,[1] G. G. Pfister,[2] M. C. Barth,[2] and G. P. Brasseur[3]

Received 26 October 2012; revised 19 December 2012; accepted 21 December 2012; published 20 February 2013.

[1] This study presents a CO source contribution analysis for the atmosphere of South Asia during January–February 2008. The approach includes into the Weather Research and Forecasting Model with Chemistry 11 CO tracers, which track CO from different source types and regions. The comparison of model results with Measurement of Pollution in the Troposphere CO retrievals shows that the model reproduces the spatial, vertical, and temporal distributions of Measurement of Pollution in the Troposphere retrievals fairly well, but generally overestimates CO retrievals in the lower troposphere. CO mixing ratios averaged over the model domain at the surface, in the planetary boundary layer, and the free troposphere are estimated as 321 ± 291, 280 ± 208, and 125 ± 27 ppbv, respectively. Model results show that wintertime CO in the boundary layer and free troposphere over India is mostly due to anthropogenic emissions and to CO inflow. In the boundary layer, the contribution from anthropogenic sources dominates (40–90%), while in the free troposphere the main contribution is due to CO inflow from the lateral boundaries (50–90%). Over the Arabian Sea and the Bay of Bengal, 43–51% of surface CO mixing ratios come from the Indian subcontinent and 49–57% from regions outside of South Asia. The anthropogenic sources in the Indo-Gangetic Plain region are found to contribute, on average, 42% and 76% to anthropogenic surface CO over the Arabian Sea and the Bay of Bengal, respectively. The anthropogenic emissions from western and southern India contribute 49% to anthropogenic surface CO over the Arabian Sea. Anthropogenic emissions contribute only up to 40% over Burma where biomass burning plays a more important role. Regional transport contributes significantly to total anthropogenic CO over southern India (41%), Burma (49%), and even exceeds the contribution from local sources in western India (58%).

Citation: Kumar, R., M. Naja, G. G. Pfister, M. C. Barth, and G. P. Brasseur (2013), Source attribution of carbon monoxide in India and surrounding regions during wintertime, *J. Geophys. Res. Atmos.*, *118*, 1981–1995, doi:10.1002/jgrd.50134.

1. Introduction

[2] Carbon monoxide (CO) is of great importance in the troposphere due to its implications on air quality, atmospheric chemistry, and global climate. Higher levels of CO in the boundary layer can lead to serious health problems [e.g., *Raub and Benignus*, 2002]. CO affects the oxidizing capacity of the atmosphere by removing the troposphere's primary oxidant, the hydroxyl (OH) radical [*Warneck*, 2000], and by influencing the tropospheric ozone budget [*Logan et al*., 1981; *Levy et al*., 1997]. It can contribute to climate change indirectly by affecting the concentrations of key greenhouse gases such as methane and ozone [e.g., *Wigley et al*., 2002]. CO with a mean tropospheric lifetime of about 2 months is also a useful tracer for tracking the transport of continental polluted air masses [e.g., *Pfister et al*., 2004; *Yashiro et al*., 2009]. Therefore, it is important to understand the different processes controlling the distribution and variability of CO in the troposphere.

[3] Numerous efforts have been made to measure CO in different chemical environments from multiple platforms including ground-, aircraft-, and satellite-based instruments [e.g., *Novelli et al*., 1992; *Drummond and Mand*, 1996; *Beer et al*., 2001; *Allen et al*., 2004]. These observations have been integrated with chemical transport models to understand the spatio-temporal variability and budget of CO in the troposphere [e.g., *Granier et al*., 1999; *de Latt et al*., 2001; *Pfister et al*., 2004]. However, such studies have been sparse over the South Asian region where anthropogenic CO emissions have been rapidly increasing (~2.3% year^{-1}) during the past 2–3 decades [*Ohara et al*., 2007] and have characteristics different from those in other parts of the world due to their disproportionately large contribution from biofuel and biomass burning [*Lawrence and Lelieveld*, 2010; *Kumar et al*., 2011].

[4] Surface CO measurements over South Asia are extremely sparse and are available only for a few sites in western

[1]Aryabhatta Research Institute of Observational Sciences, Nainital 263129, India.
[2]Atmospheric Chemistry Division, NCAR, Boulder, Colorado, 80307-3000, USA.
[3]Climate Service Center, Helmholtz Zentrum Geesthacht, Hamburg, 20146, Germany.

Corresponding author: N. Manish, Aryabhatta Research Institute of Observational Sciences, Nainital 263129, India, ARIES, Manora Peak, Nainital, Uttarakhand, 263129, India. (manish@aries.res.in)

2169-897X/13/10.1002/jgrd.50134

[*Lal et al*., 2000; *Naja et al*., 2003; *Beig et al*., 2007], southern [*Naja and Lal*, 2002; *Kumar et al*., 2008], and northern [*Aneja et al*., 2001; *Ojha et al*., 2012] parts of India. Few short-term campaign observations of surface CO are available over the adjoining oceanic regions of the Arabian Sea and the Bay of Bengal [e.g., *Naja et al*., 1999; *Lelieveld et al*., 2001; *Naja et al*., 2004; *Lal et al*., 2007; *David et al*., 2011]. These surface observations provide important information about CO seasonality and show that CO levels in South Asia are highest during winter. Measurements of the vertical distribution of CO do not exist over South Asia.

[5] Due to scarcity of in situ observations, the uses of satellite observations together with models are highly essential. Different ground- and satellite-based observations show that levels of other trace species such as ozone, NO_x, nonmethane hydrocarbons [e.g., *Lal et al*., 2000; *Sahu and Lal*, 2006; *Ghude et al*., 2008; *Kar et al*., 2010; *Kumar et al*., 2010] and aerosols [*Tripathi et al*., 2005; *Di Girolamo et al*., 2004] are also higher during winter over South Asia. Furthermore, the observations over the marine regions suggest that pollutants from inland South Asian regions can be transported to the cleaner oceanic regions during winter [e.g., *Naja et al*., 2004; *Lal et al*., 2007]. For these reasons, the present study focuses on the winter season and attempts to identify the major processes contributing to wintertime CO mixing ratios in the troposphere of South Asia and the role of regional-scale transport in distributing CO emitted from different South Asian regions.

[6] The budget of CO in the troposphere is controlled by a combination of physical and chemical processes including emissions, deposition, transport, and photochemistry. CO is emitted by both natural and anthropogenic sources but global total CO emissions are dominated by the latter [e.g., *Granier et al*., 2000; *Horowitz et al*., 2003]. The individual contributions of different processes to the CO budget have been determined in several studies by including CO tracers into global and regional models [e.g., *Granier et al*., 1999; *Lamarque and Hess*, 2003; *Pfister et al*., 2004, 2011; *Huang et al*., 2010]. This concept has also been used to quantify the contribution of different emission sources to total CO over the Indian Ocean during the Indian Ocean Experiment [*de Laat et al*., 2001]. However, such a study has not been conducted over India. More recently, this tracer concept has been successfully implemented in the Weather Research and Forecasting Model with Chemistry (WRF-Chem) to study the CO budget over the USA [*Pfister et al*., 2011; *Boynard et al*., 2012].

[7] To study the wintertime CO source contribution and variability over South Asia, the concept of CO tracers is applied with version 3.3.1 of the WRF-Chem model. An extensive comparative analysis of WRF-Chem results with observational data from surface-based, balloon-borne and space-borne sensors [*Kumar et al*., 2012a, 2012b] showed that the model can capture many important features of the trace gases observations in the South Asia region. The model reproduced the seasonal variability of CO observed at three sites in India and spatio-temporal variability of the Measurement of Pollution in the Troposphere (MOPITT) CO retrievals during all the seasons. The present manuscript begins with a description of the WRF-Chem model and different CO tracers in section 2. Section 3 illustrates the ability of the model to reproduce the spatial, temporal, and vertical structure of tropospheric CO through comparison with MOPITT retrievals. The contribution of CO from different sources and the role of regional meteorology in distributing CO over South Asia are discussed in section 4 Results from this study are summarized in section 5.

2. The Model Description

[8] This study uses version 3.3.1 of the Weather Research and Forecasting Model [*Skamarock et al*., 2008] coupled with Chemistry [*Grell et al*., 2005]. The meteorology and chemistry in the WRF-Chem model are simulated simultaneously using the mass and scalar conserving flux form of the governing equations and a terrain-following mass vertical coordinate. Both the meteorology and chemistry components of the model use the same transport scheme, grids in horizontal and vertical directions, and physical parameterizations for subgrid scale processes. In this study, the model domain is centered at 25°N, 80°E covering nearly the entire South Asian region (5°N–40°N; 60°E–100°E) at a horizontal resolution of 45 km 45 km from the surface to 10 hPa with (90,90,51) grid points in (x,y,z) directions. Different schemes used for the parameterization of atmospheric processes in the WRF-Chem configuration used for this study are listed in Table 1. The gas phase chemistry is represented by the Regional Acid Deposition Model, which includes 63 gas-phase species, 21 photolysis, and 136 gas-phase reactions [*Stockwell et al*., 1990]. The initial and boundary conditions for meteorological and chemical fields are obtained from 6 hourly National Centers for Environmental Prediction final analysis fields (http://dss.ucar.edu/datasets/ds083.2/data/) and Model for Ozone and Related Chemical Tracers – Version 4 (MOZART-4) results [*Emmons et al*., 2010], respectively.

[9] Anthropogenic emissions of CO, NO_x, SO_2, and nonmethane volatile organic compounds (NMVOCs) are taken from the Intercontinental Chemical Transport Experiment – phase B inventory [*Zhang et al*., 2009] and the Reanalysis of Tropospheric Chemical Composition (RETRO) (http://retro.enes.org/index.shtml) database as described in *Kumar et al*. [2012b]. The spatial distribution of average wintertime (December, January, and February (DJF)) anthropogenic CO emissions over the model domain used here is shown in Figure 1. Anthropogenic CO emissions are highest over the Indo-Gangetic Plain (IGP) region and other megacities (e.g., Ahmedabad, Mumbai, Delhi, Dhaka, Kolkata, and

Table 1. WRF-Chem Configuration Used in This Study

Atmospheric Process	Scheme Used
Cloud nicrophysics	Thompson microphysics [*Thompson et al*., 2004]
Long-wave radiation	Rapid Radiative Transfer Model [*Mlawer et al*., 1997]
Short-wave radiation	Goddard shortwave [*Chou and Suarez*, 1994]
Surface layer	Monin-Obukhov (Janjic Eta) [*Janjic*, 1996]
Land surface model	Noah Land Surface Model [*Chen and Dudhia*, 2001]
Planetary boundary layer	Mellor-Yamada-Janjic [*Janjic*, 1996, 2002]
Cumulus	Kain-Fritsch [*Kain*, 2004]
Photolysis	Fast-J photolysis [*Wild et al*., 2000]
Gas phase chemistry	RADM2 [*Stockwell et al*., 1990]
Dry deposition	Wesely [*Wesley*, 1989]

RADM, Regional Acid Deposition Model.

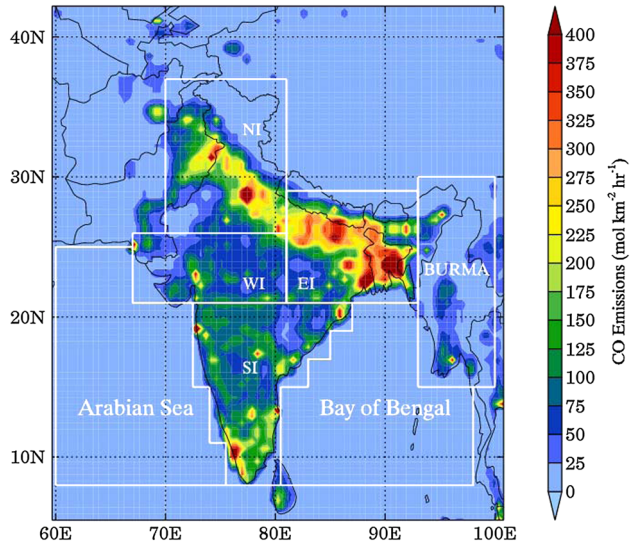

Figure 1. Spatial Distribution of wintertime (DJF) average anthropogenic CO emissions over the model domain. Regional classification of different geographical regions along with the Arabian Sea and the Bay of Bengal is also shown. NI, WI, EI, and SI represent northern, western, eastern, and southern India, respectively.

Thiruvanantpuram). CO anthropogenic emissions summed over the model domain during winter are estimated as 28,740 Gg CO. A major component of the CO anthropogenic emissions comes from biofuel use, which contributes 41% to the total anthropogenic emissions. The contributions from industrial, transportation and power plants sectors are estimated as 30%, 28%, and 1%, respectively. Biogenic emissions of trace gases from terrestrial ecosystems are calculated online from the Model of Gases and Aerosols from Nature [*Guenther et al*., 2006], but biogenic emissions of CO can be regarded as a minor source (~400 Gg/yr; http://eccad.sedoo.fr) . The emissions from biomass burning are obtained from the Fire Inventory from National Center for Atmospheric Research [*Wiedinmyer et al*., 2011] and are distributed in the model vertically following the online plume-rise module [*Freitas et al*., 2007]. Biomass burning is a small contribution during wintertime and total biomass burning CO emissions over the model domain for the considered time period are estimated as 2471 Gg.

[10] This study includes 11 CO tracers to keep track of CO contributions from different source types and geographical regions. These tracers are synthetic tracers added as individual species to the simulation and experience the same transport, chemical, and loss processes as the total simulated CO. We include tracers for CO emitted from regional anthropogenic (CO-ANT), biogenic (CO-BIO), and biomass burning (CO-BB) sources, CO produced photochemically within the domain from regional emissions of hydrocarbons (CO-CHEM) and CO inflow from the lateral domain boundaries (CO-BC). These five tracers account for all possible sources of tropospheric CO in the model. The CO-BC includes contributions from all the emission (natural as well as anthropogenic) and photochemical sources located outside the selected domain and therefore its distribution will provide information about background CO levels in this region. In addition to these five tracers, the anthropogenic emissions from five different geographical regions within the domain, namely northern India (NI), western India (WI), eastern India (EI), southern India (SI), and Burma (BUR) are tagged separately. These regions represent the largest surface emitters of anthropogenic pollution (including CO) within the model domain and are shown in Figure 1. Anthropogenic emissions of CO from outside these five regions are also tagged separately and are classified as others (OTH). Regional anthropogenic CO tracers are defined as CO-ANI, CO-AOTH etc. This is the first time that CO tracers from different regions in South Asia have been included in a regional chemistry model allowing for attribution of CO anthropogenic sources from different Indian regions. Each tagged CO undergoes the same chemical processes as the standard CO species and is deposited at the surface with the same deposition velocity. The initial and lateral boundary conditions for all the tracers are set to zero except the boundary conditions for CO-BC which are set equal to CO from MOZART.

[11] The model simulation starts on 1 December 2007 0000 UTC with a time step of 180 s, and results are output every hour. The model results can be used for source contribution analysis only after sufficient spin-up, i.e., when the sum of tagged CO tracers equals the total CO tracer. In the free troposphere, all the tracers are found to spin up well after 10 days of model run. At the surface, the percentage differences between the instantaneous total CO and the sum of CO tracers (CO_{trac} = CO-ANT + CO-BIO + CO-BB + CO-CHEM + CO-BC) show that the sum of all tracers approaches total CO values after about 20 days (Figure 2) with values within ±5% of total CO surface over the continental region of South Asia. It is 10–15% over the Oceanic region (Arabian Sea). The tracers are well spun up at the surface after 31 days with percent difference of less than ±2% over the domain and remaining within ±2% throughout the simulation. In order to avoid the effects due to spin-up, the analysis of the model results is limited to the period from 1 January to 29 February 2008.

3. Model Evaluation

[12] The model results have been evaluated extensively with ground-based, balloon-borne, and satellite-borne observations [*Kumar et al*., 2012b]. They showed that WRF-Chem results reproduced seasonal variations of ozone and CO, but deviated from NO_x measurements. Here, we extend the evaluation to focus on the January–February 2008 time period using MOPITT data. The MOPITT version 4.0 Level 2 retrievals of total column and vertical profiles of CO mixing ratios [*Deeter et al*., 2010] are used here to evaluate the model performance in simulating spatial, vertical and temporal distributions of tropospheric CO. MOPITT retrievals provide CO mixing ratios at 10 pressure levels between the surface and 100 hPa with a spacing of 100 hPa. The MOPITT retrieval algorithm uses thermal infrared radiation (near 4.7 μm) measurements in conjunction with a maximum a posteriori optimal estimation approach [*Deeter et al*., 2003; *Rodgers*, 2000]. MOPITT V4 retrievals have been extensively validated against observations from different chemical environments and are shown to have a bias of less than ±10% at all levels [*Emmons et al*., 2009; *Deeter et al*., 2010]. Here, we use only daytime MOPITT retrievals with degrees of freedom for signal greater than 1 because daytime retrievals have better information content than nighttime data [*Deeter et al*., 2010]. For comparison of model output and MOPITT, the model

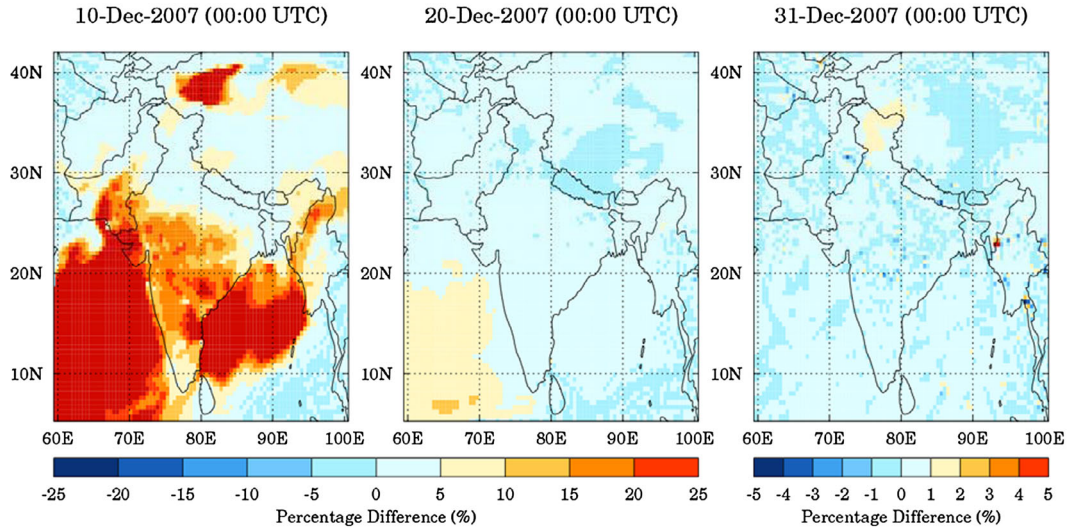

Figure 2. Spatial distribution of the percentage difference between total CO and sum of CO tracers (COtrac = CO-ANT + CO-BIO + CO-BB + CO-CHEM + CO-BC) at the surface on 10, 20, and 31 December 2007 at 00:00 UTC. The model simulation starts at 1 December 2007 at 00:00 UTC. Note the difference in color scale for 31 December 2007 when percentage differences are within ±1% in most parts of the region.

profile is first interpolated to the time and location of the selected MOPITT retrievals and the interpolated model profile is then transformed by applying the averaging kernel and a priori profile associated with the corresponding MOPITT retrieval following *Emmons et al*. [2009]. The transformed profile is denoted as WRF-Chem (AK) and represents the model profile which MOPITT would measure in absence of other errors.

[13] The spatial distributions of MOPITT and WRF-Chem (AK) total column CO averaged from 1 January to 29 February 2008 along with the percentage difference are shown in Figure 3. Both MOPITT and model show similar spatial distributions with highest CO values ($>3{\cdot}10^{18}$ molecules cm^{-2}) in the regions of highest anthropogenic CO emissions (eastern India and Bangladesh; Figure 1). Relatively higher CO column amounts ($> 2.5{\cdot}10^{18}$ molecules cm^{-2}) are also seen over South India, Burma and coastal regions of the Arabian Sea and the Bay of Bengal. The MOPITT and WRF-Chem (AK) total column CO averaged over the entire domain during January–February 2008 is estimated as $(2.4 \pm 0.2){\cdot}10^{18}$ and $(2.5 \pm 0.3){\cdot}10^{18}$ molecules cm^{-2}, respectively with a mean bias of $(9.1 \pm 19.5){\cdot}10^{16}$ molecules cm^{-2} ($4 \pm 8\%$) and a

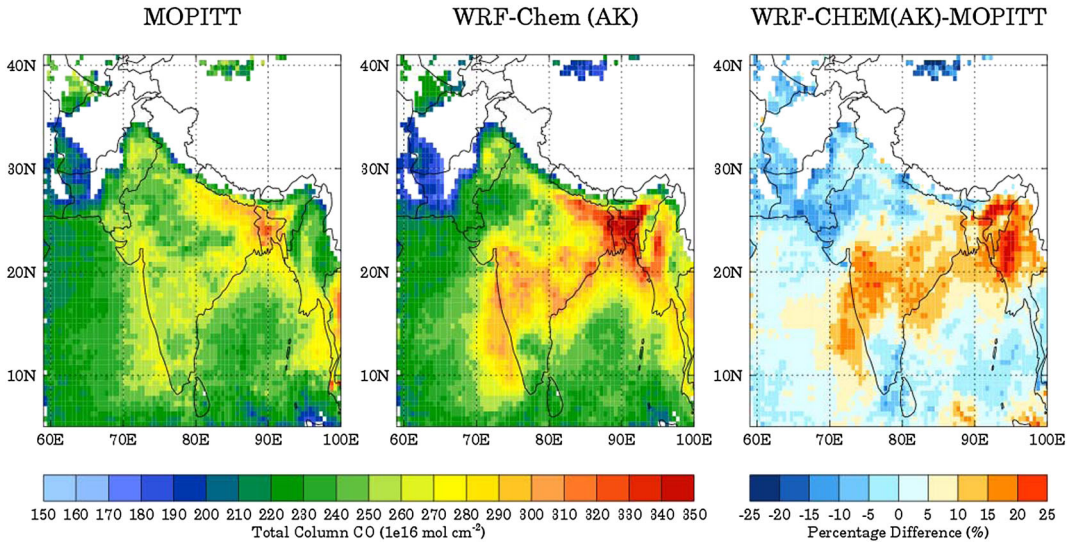

Figure 3. Spatial distribution of average CO total column retrieved from MOPITT and the corresponding WRF-Chem (AK) column (simulated column convolved with MOPITT averaging kernel) during January–February 2008. Percentage difference between model and MOPITT is also shown. The comparison includes only MOPITT daytime retrievals with degrees of freedom for signal more than 1. The white space indicates regions without valid data.

correlation coefficient of 0.82. The percentage difference between MOPITT and model CO column is within ±15% over most of the domain, except over Burma and northeastern states of India where the differences reach up to about 25%. The percentage difference plot (Figure 3) indicates that the model underestimates MOPITT CO total column over northern, western and some parts of southern India, while it overestimates satellite retrieved CO over other regions.

[14] The WRF-Chem (AK) profiles are compared with corresponding MOPITT retrieved vertical profiles of CO in Figure 4 over the seven geographical regions defined in Figure 1. The inland regions represent regions of varying anthropogenic and biomass burning emission strength, and the Arabian Sea and the Bay of Bengal represent clean marine regions with negligible emissions. The vertical distributions and gradients of CO mixing ratios are reproduced fairly well by the model over all the regions and the average model and MOPITT values match within one standard deviation at all pressure levels. Both model and MOPITT show that CO mixing ratios below 700 hPa are significantly higher than those above 700 hPa. The absolute difference between model and MOPITT varies from region to region. Except over northern India, the model generally overestimates MOPITT CO retrievals below 400 mb. The largest differences are seen over eastern India, southern India and Burma where

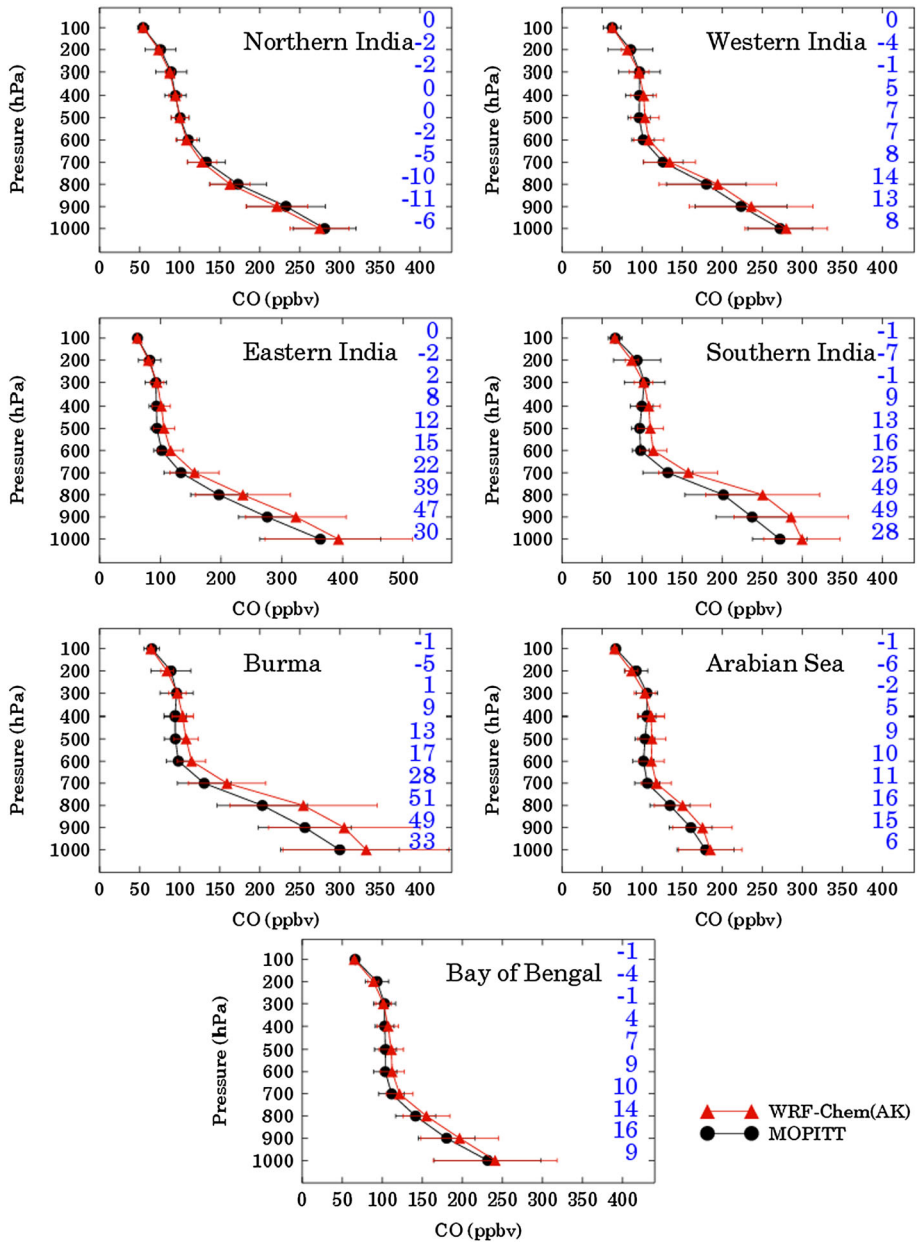

Figure 4. Vertical profiles of average CO retrieved from MOPITT and the corresponding WRF-Chem (AK) profiles during January–February 2008 over seven geographical regions defined in Figure 1. The horizontal bars represent standard deviation in the mean values. Absolute difference between model and MOPITT for each level is also shown along right *Y*-axis.

mean biases reach up to 50 ppbv at some levels in the lowermost troposphere. This indicates that overestimation of MOPITT total column CO (Figure 3) by the model over these regions is mainly due to positive biases in the lowermost troposphere and could be associated with uncertainties in model emission estimates. The anthropogenic emission estimates for CO show large variability among different available emissions inventories and range from about 55 to 86 Tg/yr for India, and from 2.5 to 7.5 Tg/yr for Burma (http://eccad.sedoo.fr). Furthermore, the errors in model transport, chemistry, physical parameterization, and uncertainty in satellite retrievals could also contribute to this discrepancy. The mean bias at all levels over other regions is generally within ±20 ppbv. It is shown later (section 4.4) that the surface CO distribution over southern parts of the domain is also affected by transport from northern and eastern India. Thus, the discrepancies between model and MOPITT over the southern regions could also result from model overestimates of CO transported from northern to southern regions. A 10 day sensitivity run is conducted to quantify the magnitude of such errors over southern regions by reducing anthropogenic CO emissions over eastern India by 25%. The comparison of base and sensitivity runs shows that a 25% reduction in eastern Indian anthropogenic CO emissions leads to a decrease of 2–10% in surface CO in downwind southern regions. The remaining differences in southern India could be attributed mainly to uncertainties in anthropogenic emissions and model transport errors.

[15] Figure 5 depicts the time series comparison of average WRF-Chem (AK) CO mixing ratios with MOPITT retrieved CO mixing ratios at 800 mb for the defined geographical regions. The comparison is shown for 800 mb because the MOPITT averaging kernel rows corresponding to 800 mb are found to peak at this level in all the regions (not shown) and thus retrievals at this level are envisaged to have higher information content. The modeled values are generally in good agreement with MOPITT retrievals and temporal variations of MOPITT retrievals are reproduced reasonably well

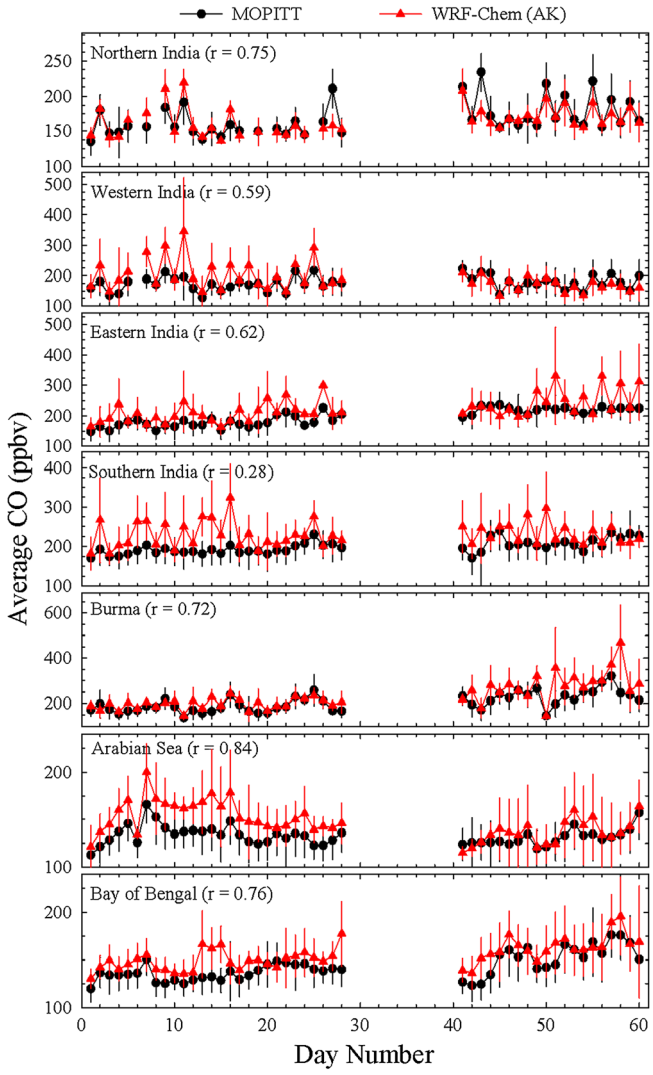

Figure 5. Time series of 25 WRF-Chem (AK) and MOPITT retrieved average CO mixing ratios at 800 mb during January–February 2008 over geographical regions defined in Figure 1. Vertical bars represent standard deviation in the mean values. The gap corresponds to missing MOPITT retrievals due to instrument calibration and decontamination activity.

by the model in all the regions with a correlation coefficient between 0.28 and 0.84. The gradual increase in CO levels over Burma and the Bay of Bengal toward the end of February is associated with the onset of biomass burning activity in Burma. The differences between model and MOPITT over the Arabian Sea are higher during January than February. Because variations in CO loading over the oceanic regions is governed mainly by transport processes, these differences could be linked to errors in anthropogenic CO emissions. The anthropogenic emissions used in the model are higher in January than February due to the application of monthly variation (derived from RETRO) to Intercontinental Chemical Transport Experiment – phase B emission inventory [*Kumar et al.*, 2012b]. This suggests that the RETRO inventory might be overestimating the monthly variation.

4. Results and Discussions

4.1. Spatial Distribution of CO

[16] The spatial distributions of total CO mixing ratios and relative contributions from different source terms (CO-ANT, CO-BB, CO-CHEM, CO-BIO, and CO-BC) at the surface and in the free troposphere (FT) are averaged over January–February 2008. Average CO mixing ratios in the FT are estimated by normalizing the FT CO column by the corresponding FT air column. The FT columns are obtained by integrating CO and air density from top of planetary boundary layer (PBL) to tropopause altitude estimated using the thermal tropopause definition [*Reichler et al.*, 2003]. The average tropopause and PBL heights during January–February 2008 along with surface altitude are shown in Figure 6 to help the interpretation. The average PBL height is 200–600 m over most of the Indian region but shows strong diurnal variability with daytime height reaching up to about 1000–3000 m and nighttime height remaining below 200 m. The average PBL height over the oceanic regions is 400–900 m with little spatial and diurnal variability. The average tropopause height is 16–17 km over regions south of 25°N and decreases sharply to about 10–11 km for 25°N to 40°N.

[17] CO mixing ratios at the surface exhibit large spatial variability (Figure 7) and are highest (> 600 ppbv) over the entire IGP region, parts of central India, southern tip of India, and southern parts of Burma. The CO-ANT distribution shows that higher CO mixing ratios over the Indian region are to a larger degree due to anthropogenic emissions. Anthropogenic CO accounts for more than 60% of total CO at the surface over India except for the high altitude Himalayan regions in northern India. Interestingly, CO-ANT also contributes significantly (30–70%) to total surface CO over the Arabian Sea and the Bay of Bengal, where anthropogenic emissions are negligible (Figure 1). This indicates the transport of CO from inland anthropogenic sources to the oceanic regions. The individual contributions of different inland regions to total anthropogenic surface CO over these oceanic regions will be quantified in section 4.4. Elevated CO mixing ratios over Burma are due to biomass burning as evident from the CO-BB distribution. CO-BB contributes 10–80% to surface CO over Burma while CO-ANT contributes 10–40%. CO-BB also contributes 5–10% to surface CO over southern India. The contributions of CO-CHEM and CO-BIO are generally less than 10% over all parts of the model domain. However, there is a clear signature of en-route photochemical production of CO over the oceanic regions in the plumes originating from Burma and India. The distribution of CO-BC shows that inflow of CO from domain boundaries generally contributes less than 40% of the total surface CO over India and Burma. CO-BC accounts for more than 60% of the total CO over the Himalayan region including the Tibetan Plateau. The distributions of total CO and all the tracers in the PBL (not shown) are also found to be similar to those at the surface.

[18] Average CO mixing ratios in the FT exhibit less spatial variability (Figure 8) and range from 90 up to 200 ppbv with highest values over the eastern IGP region, central India and Burma. The smaller spatial variability in the FT is expected due to reduced influences from surface emissions and relatively faster mixing of CO due to higher wind speeds aloft. The main (>40%) contributor to FT CO is from inflow from the boundaries as evident from CO-BC distribution. CO-ANT and CO-BB distributions show that anthropogenic and biomass burning emissions at the surface can be transported to the free troposphere in the vicinity of strong sources. These distributions also show that higher CO levels

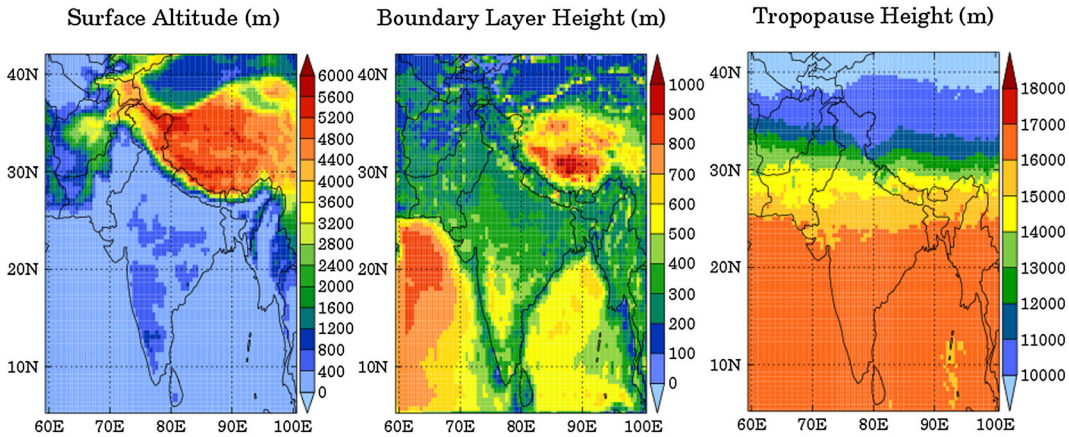

Figure 6. Spatial distribution of surface elevation, average boundary layer height and average tropopause height over the model domain during January–February 2008.

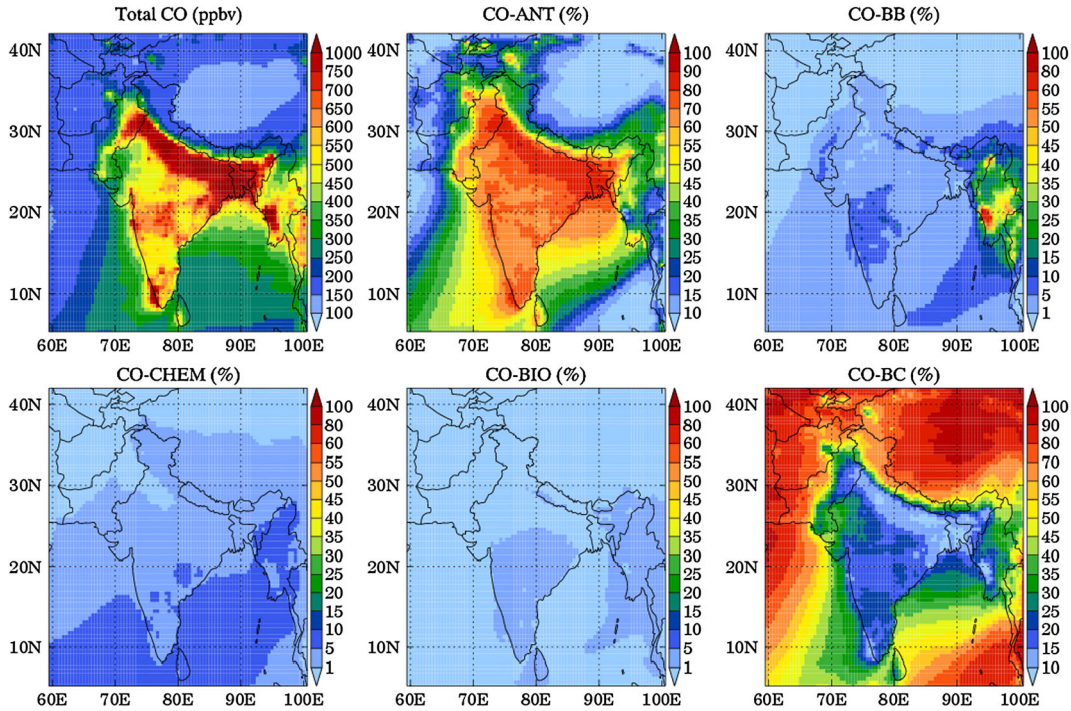

Figure 7. Surface spatial distributions of average total CO mixing ratios (ppbv) and relative contributions of CO-ANT (%), CO-BB (%), CO-CHEM (%), CO-BIO (%), and CO-BC (%) to total CO during January–February 2008. Note the variation in color scales among the graphs.

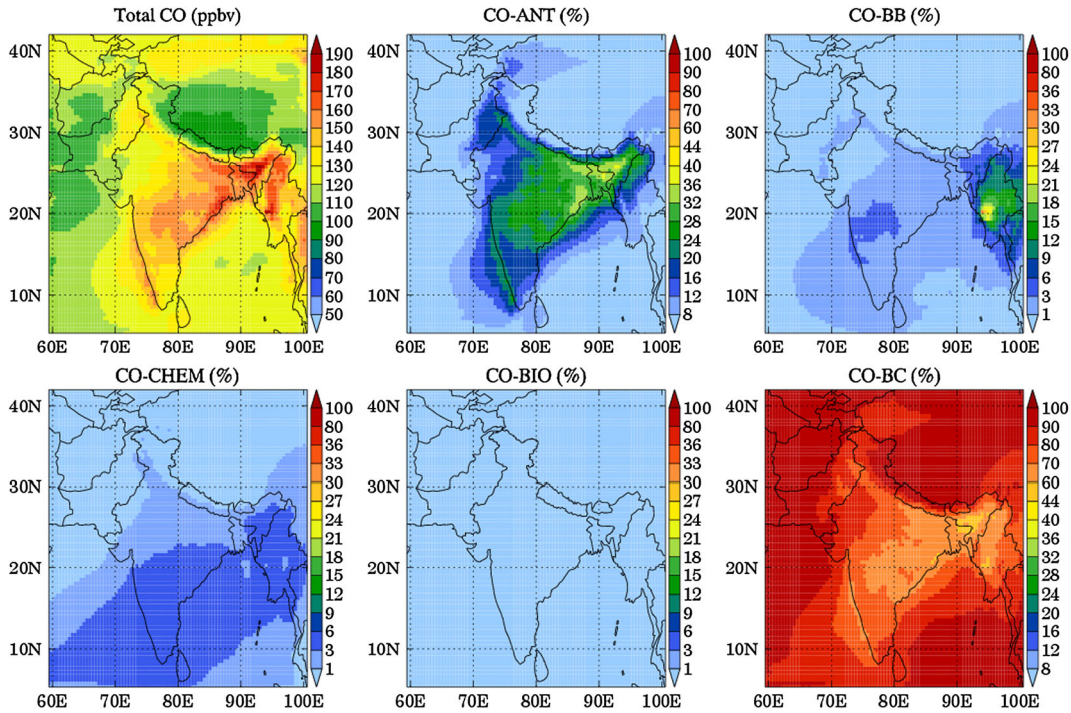

Figure 8. Free troposphere spatial distributions of average total CO mixing ratios (ppbv) and relative contributions of CO-ANT (%), CO-BB (%), CO-CHEM (%), CO-BIO (%), and CO BC (%) to total CO during January–February 2008. Note the variation in color scales among the graphs. The free troposphere is defined as the average CO amount between the top of PBL and tropopause altitude.

in the FT over eastern IGP and central India are due to the addition of anthropogenic CO (24–36%) to the CO inflow, while those over Burma are due to the addition of CO emitted from biomass burning (12–24%). In contrast to the distribution at the surface, the contribution of CO-ANT to FT CO is very small over the oceanic regions indicating that transport of CO from inland to oceanic regions occurs mainly in the boundary layer. The contribution of CO-CHEM to FT CO is less than 9% and the CO-BIO distribution highlights that biogenic emissions do not influence FT strongly and contribute less than 1%.

4.2. CO Source Attribution Analysis

[19] This section presents the source attribution analysis of CO at the surface, in the PBL and FT for the entire domain and the regions defined in Figure 1. CO mixing ratios from different source terms averaged at the surface, in the PBL and FT over the entire domain during January–February 2008 are shown in Figure 9. Average total CO mixing ratios at the surface are estimated as 321 ± 291 ppbv out of which 156 ± 243 ppbv ($34 \pm 27\%$) are provided by anthropogenic sources (CO-ANT), 134 ± 49 ppbv ($60 \pm 30\%$) by CO inflow from the domain boundaries (CO-BC), 18 ± 140 ppbv ($3 \pm 7\%$) by biomass burning (CO-BB), 11 ± 13 ppbv ($3 \pm 3\%$) by chemistry (CO-CHEM), and 3 ± 4 ($1 \pm 1\%$) by biogenic sources (CO-BIO). The average total CO mixing ratios in the PBL (280 ± 208 ppbv) and the contributions from different sources are found to be somewhat similar to those at the surface and are estimated as 120 ± 176 ppbv ($30 \pm 25\%$) for CO-ANT, 133 ± 48 ppbv ($63 \pm 29\%$) for CO-BC, 14 ± 85 ppbv ($3 \pm 7\%$) for CO-BB, 10 ± 12 ppbv ($3 \pm 3\%$) for CO-CHEM, and 2 ± 3 ppbv ($1 \pm 1\%$) for CO-BIO. The average total CO mixing ratios in the FT (125 ± 27 ppbv) are lower and have much less variance than those at the surface and in the PBL, and are mainly influenced by CO inflow from the domain boundaries as indicated by a higher average contribution of 108 ± 14 ppbv ($89 \pm 13\%$) from CO-BC. The average CO mixing ratios for other CO tracers in the FT are much lower and estimated as 12 ± 19 ppbv ($8 \pm 11\%$) for CO-ANT, 2 ± 8 ppbv ($1 \pm 3\%$) for CO-BB, 2 ± 3 ppbv ($1 \pm 1\%$) for CO-CHEM, and 0.3 ± 0.4 ppbv ($0.2 \pm 0.3\%$) for CO-BIO.

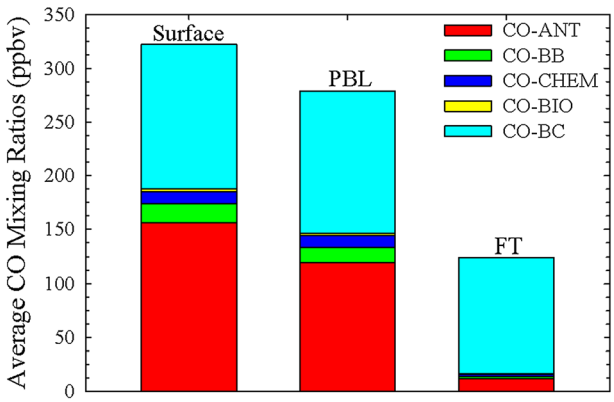

Figure 9. CO mixing ratios averaged at the surface, in the PBL and in the FT over the entire model domain during January–February 2008.

[20] The CO sources are also analyzed for the seven geographical regions defined in Figure 1. The mixing ratios of total CO and different CO tracers averaged at the surface over these regions are depicted in Table 2 along with relative contributions of each tracer to total CO mixing ratios. Anthropogenic sources (CO-ANT) provide more than 65% (159–571 ppbv) of the total surface CO over the Indian regions, while CO-BC contributes 17%–31% (110–120 ppbv). The contribution of other sources remains less than 5% over the Indian regions. Over Burma, biomass burning (24%) also emerges as an important source in addition to anthropogenic sources (36%) and CO inflow from domain boundaries (33%). Average total surface CO mixing ratios over the Arabian Sea (233 ± 71 ppbv) and the Bay of Bengal (317 ± 54 ppbv) are significantly lower than those over land regions and are mainly a result of CO from regions outside South Asia and (49–57%) and from South Asian anthropogenic sources (37–40%).

[21] Higher surface CO values over the Bay of Bengal than the Arabian Sea are consistent with previous observations of different trace species in these oceanic regions [e.g., *Lal et al.*, 2007; *Kedia and Ramachandran*, 2008; *Nair et al.*, 2008; *Srivastava et al.*, 2011]. The MOPITT retrieved CO mixing ratios averaged over the Bay of Bengal (143 ± 14 ppbv) at 800 mb are also found to be higher than the

Table 2. Mixing Ratios (ppbv) of Total CO and Different CO Tracers Averaged at the Surface During January–February 2008 Over the Seven Geographical Regions Defined in Figure 1. The Percentage Contribution of Each Tracer to Total CO Mixing Ratio Is Also Given in Parentheses. All Numbers Are Rounded-off to the Nearest Whole Number Value

Region	Total CO[a]	CO-ANT[a]	CO-BB[a]	CO-CHEM[a]	CO-BIO[a]	CO-BC[a]
Northern India	400 ± 96	270 ± 95	7 ± 5	4 ± 2	2 ± 1	118 ± 7
		(65 ± 9)	(2 ± 1)	(1 ± 1)	(-)	(31 ± 9)
Western India	473 ± 123	326 ± 122	15 ± 8	10 ± 5	5 ± 2	117 ± 7
		(67 ± 9)	(3 ± 2)	(2 ± 1)	(1 ± 0)	(27 ± 8)
Eastern India	724 ± 182	571 ± 176	21 ± 19	14 ± 5	7 ± 2	111 ± 7
		(78 ± 6)	(3 ± 2)	(2 ± 1)	(1 ± 0)	(17 ± 5)
Southern India	554 ± 145	387 ± 136	26 ± 14	20 ± 5	8 ± 2	112 ± 10
		(68 ± 7)	(5 ± 2)	(4 ± 1)	(1 ± 0)	(22 ± 6)
Burma	463 ± 162	159 ± 46	133 ± 153	21 ± 5	9 ± 2	140 ± 29
		(36 ± 11)	(24 ± 16)	(5 ± 1)	(2 ± 1)	(33 ± 10)
Arabian Sea	233 ± 71	99 ± 63	6 ± 5	9 ± 6	1 ± 1	117 ± 8
		(37 ± 15)	(2 ± 1)	(3 ± 1)	(-)	(57 ± 18)
Bay of Bengal	317 ± 54	132 ± 42	17 ± 17	17 ± 5	3 ± 1	148 ± 30
		(40 ± 15)	(5 ± 5)	(5 ± 1)	(1 ± 0)	(49 ± 11)

[a]Mean $\pm$ 1 sigma.

corresponding values over the Arabian Sea (133 ± 10 ppbv) indicating that this feature is also seen in space-borne observations of lower tropospheric CO. The analysis of different tracers shows that the contributions of CO-ANT, CO-BB, CO-CHEM and CO-BC to total CO over the Bay of Bengal are higher than those over the Arabian Sea. This suggests that the Bay of Bengal is more strongly affected by the regional sources and en-route photochemistry than the Arabian Sea. Higher CO-BC values over the Bay of Bengal are likely due to transport from Southeast Asia as evident from Figure 7 and general wind patterns over this region. The statistics for total CO and different tracers in the PBL is found to be similar to that estimated for the surface. In the FT, average total CO mixing ratios ranges from 120 to 143 ppbv over different regions with more than 75% of CO provided by CO inflow from domain boundaries and 10–21% by anthropogenic sources.

4.3. Vertical Distribution of CO

[22] The time series of the vertical distributions of total CO and different CO tracers averaged over eastern India and the Bay of Bengal from 1 January to 29 February 2008 are depicted

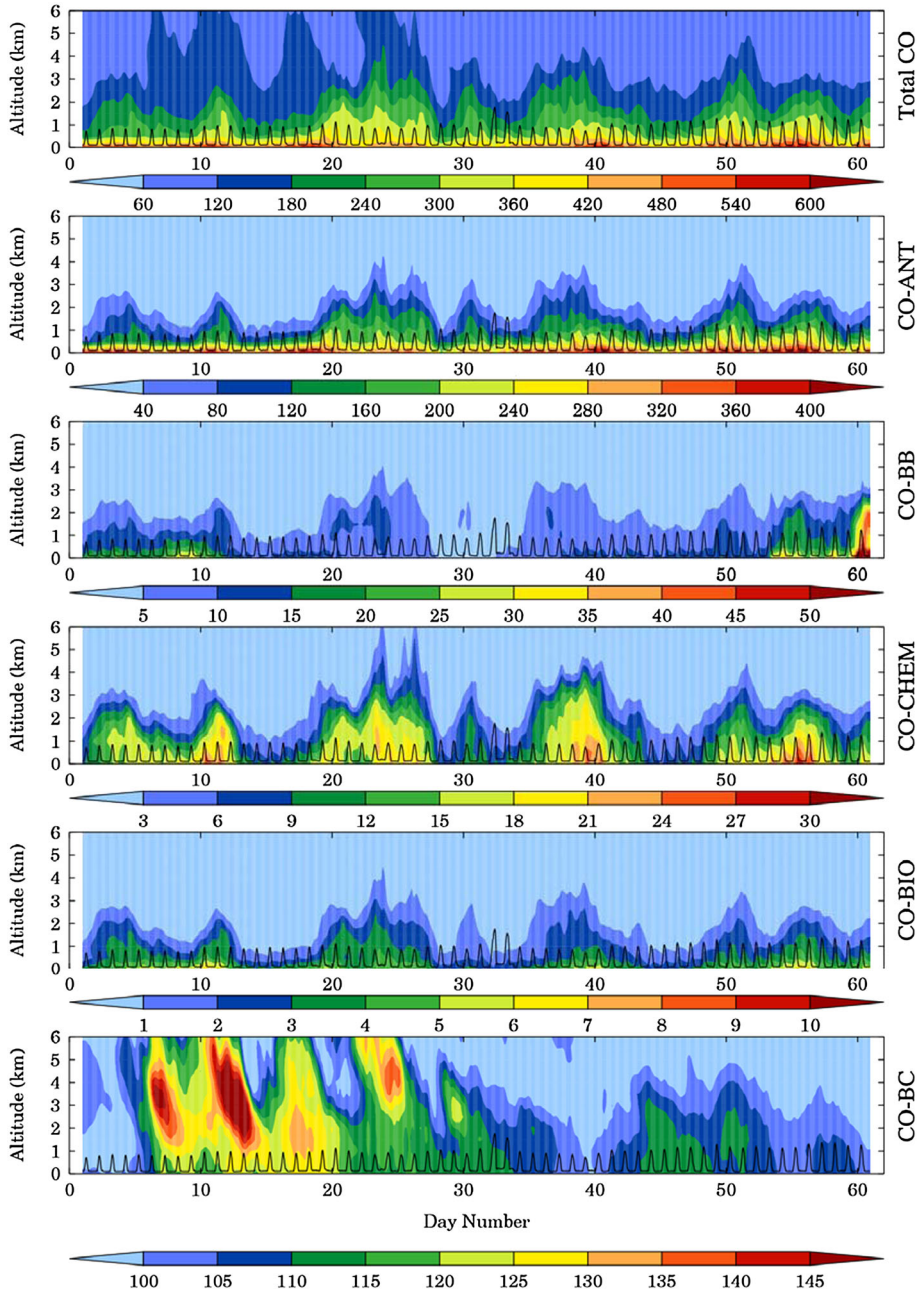

Figure 10. Vertical distribution of total CO and different CO tracers averaged over Eastern India from 1 January to 29 February 2008. Note that Eastern India is the region of highest anthropogenic emissions in the model domain and all values are in ppbv. Time series of PBL height averaged over Eastern India is also shown by solid black lines.

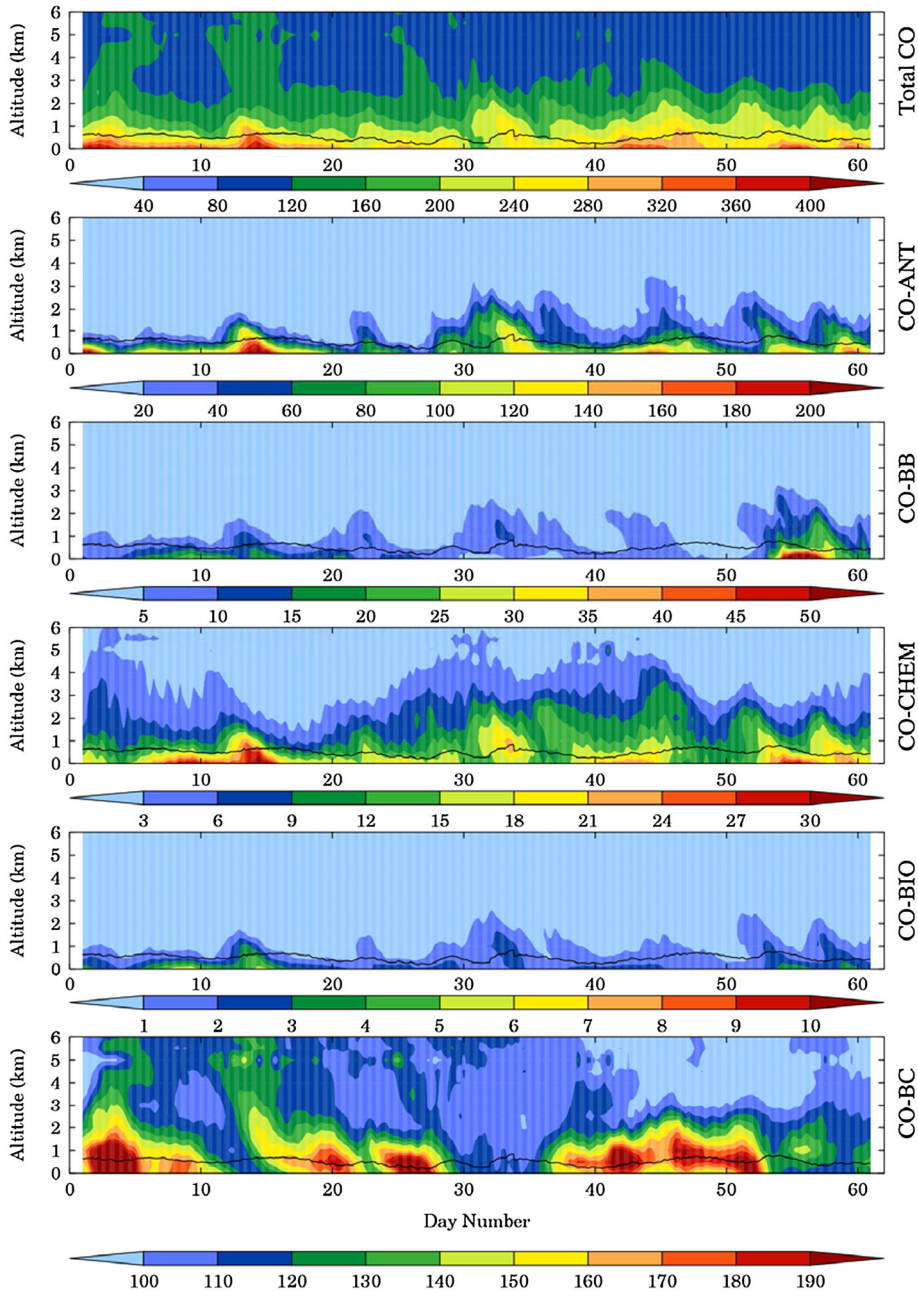

Figure 11. Vertical distribution of total CO and different CO tracers averaged over the Bay of Bengal from 1 January to 29 February 2008. All values are shown in ppbv. Time series of PBL height averaged over the Bay of Bengal is also shown by solid black lines.

in Figures 10 and 11, respectively. The eastern India and the Bay of Bengal regions are chosen to represent different chemical environments over the model domain with the former continental region with highest anthropogenic CO emissions and the latter a marine region with negligible anthropogenic CO emissions (Figure 1). The time series of average PBL height is also shown in each plot. The PBL height over eastern India varies from ~90 m during nighttime to ~1750 m during daytime reflecting the rapid response of land masses to the diurnal heating cycle, while it remains nearly constant over the Bay of Bengal. However, the simulated PBL height is dependent on the parameterization used in the model configuration.

[23] CO mixing ratios show a sharp vertical gradient over eastern India with significantly higher values in the PBL (350–600 ppbv) than in the FT (100–350 ppbv). The mixing ratios of total CO, CO-ANT, and CO-BIO in the PBL show a strong diurnal cycle with higher values during nighttime and lower values during daytime. Note that anthropogenic emissions in the model do not have a diurnal cycle and so these diurnal variations are likely due to trapping of CO molecules in the nighttime shallow boundary layer and substantial mixing into a larger volume during daytime. CO-Chem shows a moderate diurnal cycle and no clear diurnal variation is seen in CO-BC and CO-BB. Similar

temporal and vertical variations in total CO and all the CO tracers are seen over other defined inland regions. The contribution of anthropogenic, biogenic and biomass burning emissions to the total CO over all the regions is generally significant only in the lowest 3 km of the atmosphere. This confinement of regional emissions in the lower atmosphere is likely due to large-scale subsidence prevailing over the model domain during the January–February period as indicated by negative values of modeled vertical velocity in the middle to upper troposphere (700–200 mb). Over Burma, CO plumes from fires are occasionally seen to reach as high as 5 km. The height reached by fire plumes in the model is determined by the thermodynamic stability of the atmospheric environment and surface heat flux released from the fire [*Freitas et al.*, 2007]. The buoyancy flux generated by the fires is directly proportional to the product of convective energy flux and the plume radius. The convective energy flux is calculated from surface heat flux while the radius of the plume is estimated by the fire size. The average fire sizes for different land-use categories in Burma are found to be higher by a factor of 0.5 to 2.3 than those for rest of the domain, which in turn would lead to a higher buoyancy flux and thus higher injection heights.

[24] The vertical distribution of total CO mixing ratios over the Bay of Bengal is similar to those observed over land regions with higher values in the PBL (180–400 ppbv) and lower values in the FT (90–250 ppbv), but the gradient is smaller and there is no clear signal of a diurnal variation in CO. This is interesting since the emissions over the Bay of Bengal are negligible and thus indicates the transport of CO from the surrounding land regions to the oceanic regions during winter. Higher values of CO-ANT, CO-BB, and CO-BIO distributions in the PBL indicate that transport of pollutants generally occur within the PBL. The en-route photochemical production also adds 10–25 ppbv to CO in the PBL over the Bay of Bengal as evident from CO-CHEM distribution. CO-BC distribution shows that CO inflow from domain boundaries also enhances CO in both the PBL and in the FT frequently by more than 150 ppbv. Higher CO-BC values over the Bay of Bengal than eastern India are due to the proximity of the former region to the domain boundaries and most likely represent anthropogenic and biomass burning emissions in Southeast Asia which are included in the MOZART-4 simulations that supply the boundary conditions to WRF-Chem.

4.4. Regional Meteorology and Anthropogenic CO Distribution

[25] In this section, we examine the transport pathways of CO emitted from anthropogenic sources located in different South Asian regions. We then quantify the relative contribution of the regional transport compared to the local anthropogenic CO emissions in each of the different regions marked in Figure 1. In the previous sections, it was shown that the anthropogenic sources significantly contribute to the CO concentrations only in the lowermost troposphere. Therefore our analysis focuses on the surface apportionment of CO from different regions. The spatial distributions of CO emitted from

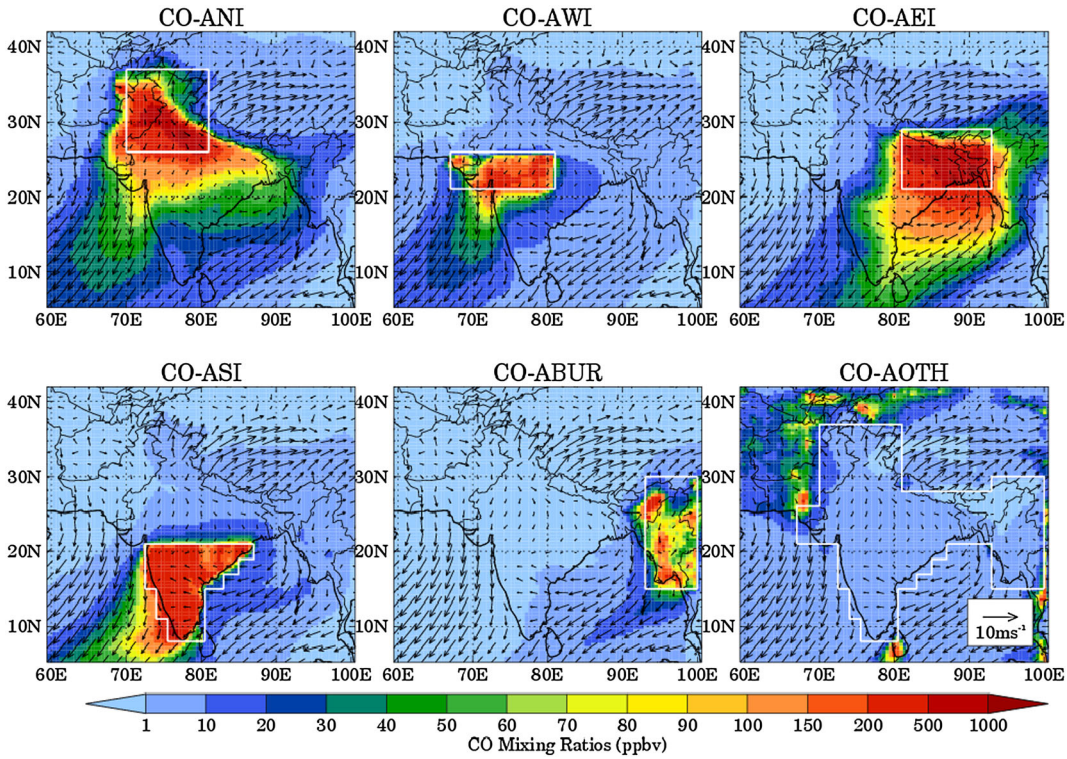

Figure 12. Spatial distribution of surface CO emitted from anthropogenic sources in Northern India (CO-ANI), Western India (CO-AWI), Eastern India (CO-AEI), Southern India (CO-ASI), Burma (CO-ABUR), and other regions (CO-OTH) averaged at the surface during January–February 2008. Average 10 m wind vectors are also shown to portray regional low level circulation. The white box shows the geographical boundaries of the respective regions.

anthropogenic sources located in northern (CO-ANI), western (CO-AWI), eastern (CO-AEI), and southern India (CO-ASI), Burma (CO-ABUR), and other regions (CO-AOTH) averaged at the surface during January–February 2008 along with averaged 10 m wind vectors are shown in Figure 12. The wind patterns indicate that the low level circulation is favorable for transport of pollutants from northern to southern parts of the model domain.

[26] The winds from northern India blow in two channels: one consisting of northwesterly winds along the Indo-Gangetic Plain region and the other one consisting of northeasterly winds blowing toward western India. Consequently, the anthropogenic sources in northern India (CO-ANI) provide CO to most parts of the domain. The CO emitted by anthropogenic sources in western India (CO-AWI) is transported by northerly winds into the Arabian Sea, from where it is transported southwestward by northeasterly trade winds. The northerly winds also transport CO emitted by eastern Indian anthropogenic sources (CO-AEI) into the Bay of Bengal and change to northeasterly/easterly as they progress southward thereby carrying eastern Indian plumes to southern India and the Arabian Sea. CO-ASI distribution shows that southern Indian anthropogenic sources largely influence the distribution in southern Arabian Sea. Anthropogenic sources in Burma (CO-ABUR) can contribute 10–20 ppbv over the Bay of Bengal. Anthropogenic emissions from other regions (CO-AOTH) contribute less than 20 ppbv to surface CO over all the Indian regions, Burma and the oceanic regions. Similar spatial distributions are seen for all these tracers, when analyzed for the PBL.

[27] The contributions of the different tracers to total anthropogenic CO at the surface over the defined seven regions is presented in Table 3. The amount of CO provided by the sources located within a given region (e.g., CO-ANI for northern India) is defined as contribution from local sources and the CO coming from sources outside this region (e.g., CO-AWI + CO-AEI + CO-ASI + CO-ABUR + CO-AOTH for northern India) represent contribution from regional transport. The local sources account for most of the total anthropogenic CO in northern (92%) and eastern (83%) India, but regional transport makes a significant contribution in southern India (41%) and Burma (49%). In western India, the regional transport contribution (58%) to CO is greater than the local emissions (42%). However, the variability of total anthropogenic CO in all the inland regions is driven mainly by local sources as indicated by the standard deviations, which are about half the magnitude of the averages. The model evaluation results (Figures 3–5) showed an overestimation of CO over western India and southern India; if northern or eastern Indian emissions are overestimated then the contribution of regional transport to CO over these regions could be smaller but still significant. Like inland regions, the Arabian Sea and the Bay of Bengal do not encompass local sources, and anthropogenic CO over these regions is mainly due to transport. It is found that the major sources of total anthropogenic CO over the Bay of Bengal come from eastern (62%) and northern India (14%) while those for the Arabian Sea come from northern (36%), western (27%) and southern India (22%). These results demonstrate the importance of regional-scale transport in distributing the anthropogenic emissions and in controlling surface CO variability in South Asia.

5. Conclusions

[28] The contribution of different sources to the tropospheric CO distribution in South Asia during January–February 2008 has been analyzed using CO tracers in the WRF-Chem. Eleven CO tracers were included in the model with five of them keeping track of CO originating from emissions sources (anthropogenic, biogenic and biomass burning), photochemistry and CO inflow from domain boundaries, and the other six tracking CO emitted from anthropogenic sources located in different geographical regions of the domain. The model performance is evaluated by comparing the model output with CO retrievals from the MOPITT instrument. The spatial, vertical and temporal distributions of MOPITT CO retrievals are fairly well reproduced by the model over different geographical regions of South Asia. However, the model generally overestimates MOPITT retrievals in the lower troposphere.

Table 3. Mixing Ratios (ppbv) of Total Anthropogenic CO and Different Anthropogenic Regional CO Tracers Averaged at the Surface During January–February 2008 Over the Seven Geographical Regions Defined in Figure 1. The Percentage Contribution of each Tracer to Total Anthropogenic CO Mixing Ratio Is Also Given in Parentheses. All Numbers Are Rounded-off to the Nearest Whole Number Value

Region	CO-ANT[a]	CO-ANI[a]	CO-AWI[a]	CO-AEI[a]	CO-ASI[a]	CO-ABUR[a]	CO-AOTH[a]
Northern India	270 ± 95	249 ± 90	3 ± 5	10 ± 13	1 ± 4	-	7 ± 2
		(92 ± 7)	(1 ± 2)	(4 ± 5)	(-)		(3 ± 1)
Western India	326 ± 122	136 ± 54	142 ± 71	30 ± 25	10 ± 14	-	8 ± 3
		(43 ± 12)	(42 ± 13)	(9 ± 7)	(3 ± 3)		(3 ± 1)
Eastern India	571 ± 176	68 ± 31	8 ± 5	476 ± 173	11 ± 9	6 ± 5	2 ± 0
		(13 ± 7)	(2 ± 1)	(82 ± 7)	(2 ± 2)	(1 ± 1)	(-)
Southern India	387 ± 136	38 ± 13	25 ± 9	76 ± 36	245 ± 111	1 ± 1	2 ± 1
		(11 ± 3)	(6 ± 2)	(22 ± 9)	(59 ± 11)	(-)	(1 ± 0)
Burma	159 ± 46	12 ± 6	4 ± 3	54 ± 32	7 ± 7	78 ± 31	3 ± 1
		(8 ± 4)	(2 ± 2)	(33 ± 14)	(4 ± 4)	(51 ± 19)	(2 ± 1)
Arabian Sea	99 ± 63	32 ± 21	23 ± 15	8 ± 9	30 ± 28	-	5 ± 2
		(36 ± 14)	(27 ± 7)	(6 ± 5)	(22 ± 14)		(9 ± 7)
Bay of Bengal	132 ± 42	19 ± 9	5 ± 4	85 ± 32	9 ± 8	10 ± 8	4 ± 2
		(14 ± 6)	(4 ± 2)	(62 ± 9)	(7 ± 6)	(9 ± 6)	(4 ± 4)

[a]Mean ± 1 sigma.

[29] The attribution of CO sources is analyzed at the surface, in the PBL and the FT. CO mixing ratios at the surface, in the PBL and the FT averaged over the entire domain are estimated to be 321, 280, and 125, respectively during January–February 2008. CO at the surface and in the PBL exhibit large spatial variability and is controlled largely by anthropogenic sources (30–34%) and CO inflow from the domain boundaries (60–63%), while CO in the FT show little spatial variability and is controlled mainly by CO inflow from the domain boundaries (89%). In Burma, biomass burning sources contribute significantly (10–80%) to total CO concentration both at the surface and in the PBL. Average mixing ratios of other tracers are less than 20 ppbv (<10%) over the model domain. The vertical distributions of CO tracers for anthropogenic, biogenic and biomass burning sources indicate that CO originating from regional emissions contributes significantly to CO concentrations only within the lowest 3 km of the atmosphere. The contribution of anthropogenic emissions to total surface CO is also found to be significant over the oceanic regions of the Arabian Sea (37%) and the Bay of Bengal (40%). The analysis of low level circulation along with regional anthropogenic CO emission tracers showed that the local sources provide most of the total anthropogenic CO over northern and eastern India, but regional transport contributes significantly to southern India and Burma, and even exceeds the contribution from local sources in western India. The major source regions contributing to anthropogenic CO over the Arabian Sea are found in northern, western and southern India while those for the Bay of Bengal are located in eastern and northern India.

[30] This study illustrates the potential of integrating satellite observations with chemistry transport modeling to understand the different processes controlling the distribution and variability of tropospheric CO over the regions of limited observations such as South Asia. However, it is imperative to conduct in situ observations of tropospheric CO concentrations as well as emissions over these regions to better evaluate the model performance and improve the CO emission estimates by supplementing the current bottom-up emission estimates with inverse modeling. Such observations should also provide more detailed information on the vertical distribution of tropospheric CO in South Asia, which currently does not exist.

[31] **Acknowledgments**. R. Kumar is thankful to Martin Claussen for his thorough support, encouragement and keen interest in this work. The authors would also like to thank the MOPITT team for providing CO retrievals. The data sets of initial and boundary conditions for meteorological fields is downloaded from the website http://dss.ucar.edu/datasets/ds083.2/data/. The data sets of initial and boundary conditions for chemical fields, biogenic emission, biomass burning emissions and programs used to process these data sets are downloaded from the website http://www2.acd.ucar.edu/wrf-chem/. The National Center for Atmospheric Research is supported by the National Science Foundation. Comments from the three reviewers were very useful in improving the manuscript and are acknowledged.

References

Allen, D., K. Pickering, and M. Fox-Rabinovitz (2004), Evaluation of pollutant outflow and CO sources during TRACE-P using model-calculated, aircraft-based, and Measurements of Pollution in the Troposphere (MOPITT)-derived CO concentrations, *J. Geophys. Res.*, *109*, D15S03, doi:10.1029/2003JD004259.

Aneja, V. P., A. Agarwal, P. A. Roelle, S. B. Phillips, Q. Tong, N. Watkins, and R. Yablonsky (2001), Measurements and analysis of criteria pollutants in New Delhi, India, *Environ. Int.*, *27*, 35–42.

Beer, R., T. A. Glavich, and D. M. Rider (2001), Tropospheric Emission Spectrometer for the Earth Observing System Aura satellite, *Appl. Opt.*, *40*, 2356–2367.

Beig, G., S. Gunthe, and D. B. Jadhav (2007), Simultaneous measurements of ozone and its precursors on a diurnal scale at a semi urban site in India, *J. Atmos. Chem.*, *57*, 239–253, doi:10.1007/s10874-007-9068-8.

Boynard, A., G. G. Pfister and D. P. Edwards (2012), Boundary layer versus free tropospheric CO budget and variability over the United States during summertime, *J. Geophys. Res.*, *117*, D04306, doi:10.1029/20011JD016416.

Chen, F., and J. Dudhia (2001), Coupling an advanced land-surface-hydrology model with Penn state-NCAR MM5 modeling system, Part I: Model implementation and sensitivity, *Mon. Wea. Rev.*, *129*, 569–585.

Chou, M.-D., and M. J. Suarez (1994), An efficient thermal infrared radiation parametrization for use in general circulation models, *NASA Tech. Memo. 104606*, *3*, 85 pp.

David, L. M., I. A. Girach, and P. R. Nair (2011), Distribution of ozone and its precursors over Bay of Bengal during winter 2009: role of meteorology, *Ann. Geophys.*, *29*, 1613–1627, doi:10.5194/angeo-29-1613-2011.

de Latt, A., J. Lelieveld, G. Roelofs, R. Dickerson, and J. Lobert (2001), Source analysis of carbon monoxide pollution during INDOEX 1999, *J. Geophys. Res.*, *106*, D22, doi:10.1029/2000JD900679.

Deeter, M. N., et al. (2003), Operational carbon monoxide retrieval algorithm and selected results for the MOPITT instrument, *J. Geophys. Res.*, *108*(D14), 4399, doi:10.1029/2002JD003186.

Deeter, M. N., et al. (2010), The MOPITT version 4 CO product: Algorithm enhancements, validation, and long-term stability, *J. Geophys. Res.*, *115*, D07306, doi:10.1029/2009JD013005.

Di Girolamo, L., et al. (2004), Analysis of Multi-angle Imaging Spectro-Radiometer (MISR) aerosol optical depths over greater India during winter 2001-2004, *Geophys. Res. Lett.*, *31*, L23115, doi:10.1029/2004GL021273.

Drummond, J. R., and G. S. Mand (1996), The Measurement of Pollution in the Troposphere (MOPITT) Instrument: Overall performance and calibration requirements, *J. Atmos. Oceanic Technol.*, *13*, 314–320.

Emmons, L. K., D. P. Edwards, M. N. Deeter, J. C. Gille, T. Campos, P. Nédélec, P. Novelli, and G. Sachse (2009), Measurements of Pollution in the Troposphere (MOPITT) validation through 2006, *Atmos. Chem. Phys.*, *9*, 1795–1803, doi:10.5194/acp-9-1795-2009.

Emmons, L. K., et al. (2010), Description and evaluation of the Model for Ozone and Related Chemical Tracers, version 4 (MOZART-4), *Geosci. Model. Dev.*, *3*, 43–67, doi:10.5194/gmd-3-43-2010.

Freitas, S. R., K. M. Longo, R. Chatfield, R. Latham, M. A. S. Silva Dias, M. O. Andreae, E. Prins, J. C. Santos, R. Gielow, and J. A. Carvalho Jr. (2007), Including the sub-grid scale plume rise of vegetation fires in low resolution atmospheric transport models, *Atmos. Chem. Phys.*, *7*, 3385–3398, doi:10.5194/acp-7-3385-2007.

Ghude, S. D., S. Fadnavis, G. Beig, S. D. Polade, and R. J. van der A (2008), Detection of surface emission hot spots, trends, and seasonal cycle from satellite-retrieved NO_2 over India, *J. Geophys. Res.*, *113*, D20305, doi:10.1029/2007JD009615.

Granier, C., G. Petron, J. -F. Mueller, and G. Brasseur (2000), The impact of natural and anthropogenic hydrocarbons on the tropospheric budget of carbon monoxide, *Atmos. Environ.*, *34*, 5255–5270.

Granier, C., J. F. Mueller, G. Petron, and G. Brasseur (1999), A three dimensional study of the global CO budget, *Chemosphere Global Change Sci.*, *1*, 255–261, doi:10.1016/S1465-9972(99)00007-0.

Grell, G. A., S. E. Peckham, R. Schmitz, S. A. Mckeen, G. Frost, W. C. Skamarock, and B. Eder (2005), Fully coupled online chemistry within the WRF model, *Atmos. Environ.*, *39*, 6957–6975, doi:10.1006/j.atmosenv.2005.04.027.

Guenther, A., T. Karl, P. Harley, C. Wiedinmyer, P. I. Palmer, and C. Geron (2006), Estimates of global terrestrial isoprene emissions using MEGAN (Model of Emissions of Gases and Aerosols from Nature), *Atmos. Chem. Phys.*, *6*, 3181–3210, doi:10.5194/acp-6-3181-2006.

Horowitz, L. W., et al. (2003), A global simulation of tropospheric ozone and related tracers: Description and evaluation of MOZART, version 2, *J. Geophys. Res.*, *108*(D24), 4784, doi:10.1029/2002JD002853.

Huang, M., et al. (2010), Impacts of transported background ozone on California air quality during the ARCTAS-CARB period: A multi-scale modeling study, *Atmos. Chem. Phys.*, *10*, 6947–6968, doi:10.5194/acp-10-6947-2010.

Janjic, Z. I. (1996), The surface layer in the NCEP Eta Model, *Eleventh Conference on Numerical Weather Prediction*, Norfolk, VA, 19–23 August, Amer. Meteor. Soc., Boston, MA, 354–355.

Janjic, Z. I. (2002), Nonsingular Implementation of the Mellor-Yamada Level 2.5 Scheme in the NCEP Meso model, *NCEP Office Note*, *437*, 61.

Kain, J. S. (2004), The Kain-Fritsch convective parameterization: An update, *J. Appl. Meteor.*, *43*, 170–181.

Kar, J., M. N. Deeter, J. Fishman, Z. Liu, A. Omar, J. K. Creilson, C. R. Trepte, M. A. Vaughan, and D. M. Winker (2010), Wintertime pollution

over the Eastern Indo-Gangetic Plains as observed from MOPITT, CALIPSO and tropospheric ozone residual data, *Atmos. Chem. Phys.*, *10*, 12273–12283, doi:10.5194/acp-10-12273-2010.

Kedia, S., and S. Ramachandran (2009), Features of aerosol optical depths over the Bay of Bengal and the Arabian Sea during premonsoon season: Variabilities and anthropogenic influence, *J. Geophys. Res.*, *113*, D11201, doi:10.1029/2007JD009070.

Kumar, G. M., S. Sampath, V. S. Jeena, and R. Anjali (2008), Carbon Monoxide Pollution Levels at Environmentally Different Sites, *J. Ind. Geophys. Union*, *12*(1), 31–40.

Kumar, R, M. Naja, S. Venkataramani, and O. Wild (2010), Variations in surface ozone at Nainital, a high altitude site in the central Himalayas, *J. Geophys. Res. 115*, D16302, doi:10.1029/2009JD013715.

Kumar, R., M. Naja, S. K. Satheesh, N. Ojha*, H. Joshi, T. Sarangi*, P. Pant, U. C. Dumka, P. Hegde, and S. Venkataramani (2011), Influences of the springtime Northern Indian biomass burning over the central Himalayas, *J. Geophys. Res. 116*, D19302, doi:10.1029/2010JD0155059.

Kumar, R., M. Naja, G. G. Pfister, M. C. Barth, and G. P. Brasseur (2012a), Simulations over South Asia using the Weather Research and Forecasting model with Chemistry (WRF-Chem): set-up and meteorological evaluation, *Geosci. Model. Dev.*, *5*, 321–343, doi:10.5194/gmd-5-321-2012.

Kumar, R., M. Naja, G. G. Pfister, M. C. Barth, C. Wiedinmyer, and G. P. Brasseur (2012b), Simulations over South Asia using the Weather Research and Forecasting model with Chemistry (WRF-Chem): chemistry evaluation and initial results, *Geosci. Model. Dev.*, *5*, 619–648, doi:10.5194/gmd-5-619-2012.

Lal, S., L. K. Sahu, and S. Venkataramani (2007), Impact of transport from the surrounding continental regions on the distributions of ozone and related gases over the Bay of Bengal during February 2003, *J. Geophys. Res.*, *112*, D14302, doi:10.1029/2006JD008023.

Lal, S., M. Naja, and B. H. Subbaraya (2000), Seasonal variations in surface ozone and its precursors over an urban site in India, *Atmos. Environ.*, *34*, 2713–2724, doi:10.1016/S1352-2310(99)00510-5.

Lamarque, J. –F., and P. G. Hess (2003), Model analysis of the temporal and geographical origin of the CO distribution during the TOPSE campaign, *J. Geophys. Res.*, *108*(D4), 8354, doi:10.1029/2002JD002077.

Lawrence, M. G., and J. Lelieveld (2010), Atmospheric pollutant outflow from southern Asia: a review, *Atmos. Chem. Phys.*, *10*, 11017–11096, doi:10.5194/acp-10-11017-2010.

Lelieveld, J., et al. (2001), The Indian Ocean Experiment: Widespread Air Pollution From South and Southeast Asia, *Science*, *291*, 1031–1036.

Levy II, H., P. S. Kasibhatla, W. J. Moxim, A. A. Klonecki, A. L. Hirsch, S. J. Oltmans, and W. L. Chameides (1997), Global impact of human activity on tropospheric ozone, *Geophys. Res. Lett.*, *24*, 791–794.

Logan, J. A., M. J. Prather, S. C. Wofsy, and M. B. McElroy (1981), Tropospheric Chemistry: A global perspective, *J. Geophys. Res.*, *86*, 7210–7254, doi:10.1029/JC086iC08p07210.

Mlawer, E. J. et al. (1997), Radiative transfer for inhomogenous atmosphere: RRTM, a validated correlated-k model for the long-wave. *J. Geophys. Res.*, *102*(D14), 16663–16682.

Nair, V. S., S. S. Babu, and K. K. Moorthy (2008), Spatial distribution and spectral characteristics of aerosol single scattering albedo over the Bay of Bengal inferred from shipborne measurements, *Geophys. Res. Lett.*, *35*, L10806, doi:10.1029/2008GL033687.

Naja, M., S. Lal, S. Venkataramani, and K. S. Modh (1999), and Duli Chand, Variabilities in O_3, NO, CO and CH_4 over the Indian Ocean during winter season. *Curr. Sci.*, *76*, 101–107.

Naja, M., and S. Lal (2002), Surface ozone and precursors gases at Gadanki (13.5°N, 79.2°E), tropical rural site in India, *J. Geophys. Res.*, *107*(D14), 4197, doi:10.1029/2001JD002477.

Naja, M., S. Lal, and D. Chand (2003), Diurnal and seasonal variabilities in surface ozone at a high-altitude site Mt. Abu (24.6°N, 72.7°E, 1680 m asl) in India, *Atmos. Environ.*, *37*, 4205–4215, doi:10.1016/S1352-2310(03)00565-X.

Naja, M., D. Chand, L. Sahu, and S. Lal (2004), Trace gases over marine regions around India, *Indian J. Mar. Sci.*, *33*(1), 95–106, IPCCode:Int. Cl7.C09K3/30.

Novelli, P. C., L. P. Steele, and P. P. Tans (1992), Mixing Ratios of Carbon Monoxide in the Troposphere, *J. Geophys. Res.*, *97*, D18, 731–750, doi:10.1029/92JD02010.

Ohara, T., H. Akimoto, J. Kurokawa, N. Horri, K. Yamaji, X. Yan, and T. Hayasaka (2007), An Asian emission inventory of anthropogenic emission sources for the period 1980-2020, *Atmos. Chem. Phys.*, *7*, 4419–4444, doi:10.5194/acp-7-4419-2007.

Ojha, N., M. Naja, K. P. Singh, T. Sarangi, R. Kumar, S. Lal, M. G. Lawrence, T. M. Butler, and H. C. Chandola (2012), Variabilities in ozone at a semi-urban site in the Indo-Gangetic Plain region: Association with the meteorology and regional process, *J. Geophys. Res.*, *117*, D20301, doi:10.1029/2012JD017716.

Pfister, G. G., J. Avise, C. Wiedinmyer, D. P. Edwards, L. K. Emmons, G. D. Diskin, J. Podolske, and A. Wisthaler (2011), CO source contribution analysis for California during ARCTAS-CARB, *Atmos. Chem. Phys.*, *11*, 7515–7532, doi:10.5194/acp-11-7515-2011.

Pfister, G., G. Pétron, L. K. Emmons, J. C. Gile, D. P. Edwards, J.-F. Lamarque, J.-L. Attie, C. Granier, and P. C. Novelli (2004), Evaluation of CO simulations and the analysis of the CO budget for Europe, *J. Geophys. Res.*, *109*, D19304, doi:10.1029/2004JD004691.

Raub, J. A., and V. A. Benignus (2002), Carbon Monoxide and the Nervous System, *Neurosci. Biobehav. Rev.*, *26*(8), 925–940.

Reichler, T., M. Dameris, and R. Sausen (2003), Determining the tropopause height from gridded data, *Geophys. Res. Lett.*, *30*(20), 2042, doi:10.1029/2003GL018240.

Rodgers, C. D. (2000), Inverse Methods for Atmospheric Sounding, Theory and Practice, World Sci, River Edge, N. J.

Sahu, L. K., and S. Lal (2006), Distributions of C2-C5 NMHCs and related trace gases at a tropical urban site in India, *Atmos. Environ.*, *40*(5), 880–891.

Skamarock, W. C., J. B. Klemp, J. Dudhia, D. O. Gill, D. M. Barker, M. Duda, X.-Y. Huang, W. Wang, and J. G. Powers (2008), A description of the Advanced Research WRF version 3, NCAR Tech. Note NCAR/TN-475 + STR, 125 pp., Natl. Cent. For Atmos. Res., Boulder, Colo.

Srivastava, S., S. Lal, S. Venkataramani, S. Gupta, and Y. B. Acharya (2011), Vertical distribution of ozone in the lower troposphere over the Bay of Bengal and the Arabian Sea during ICARB-2006: Effects of continental outflow, *J. Geophys. Res.*, *116*, D13301, doi:10.1029/2010JD015298.

Stockwell, W. R., P. Middleton, J. S. Chang, and X. Tang (1990), The second Generation Regional Acid Deposition Model Chemical Mechanism for Regional Air Quality Modeling, *J. Geophys. Res.*, *95*(D10), 16343–16367, doi:10.1029/JD095iD10p16343.

Thompson, G., R. M. Rasmussen, and K. Manning (2004), Explicit forecasts of winter precipitation using an improved bulk microphysics scheme. Part I: Description and sensitivity analysis, *Mon. Wea. Rev.*, *132*, 519–542.

Tripathi, S. N., S. Dey, V. Tare, and S. K. Satheesh (2005), Aerosol black carbon radiative forcing at an industrial city in Northern India, *Geophys. Res. Lett.*, *32*, L08802, doi:10.1029/2005GL022515.

Warneck, P. (2000), Chemistry of the Natural Atmosphere, 927 pp., Academic, San Diego, California.

Wesley, M. L. (1989), Parameterization of surface resistance to gaseous dry deposition in regional numerical model, *Atmos. Environ.*, *16*, 1293–1304.

Wiedinmyer, C., S. K. Akagi, R. J. Yokelson, L. K. Emmons, J. A. Al-Saadi, J. J. Orlando, and A. J. Soja (2011), The Fire Inventory from NCAR (FINN): A high resolution global model to estimate the emissions from open burning, *Geosci. Model Dev.*, *4*, 625–641, doi:10.5194/gmd-4-625-2011.

Wigley, T. M. L., S. J. Smith, and M. J. Prather (2002), Radiative forcing due to reactive gas emissions, *J. Clim.*, *15*(18), 2690–2696, doi:10.1175/1520-0442(2002)015<2690: RFDTRG>2.0.CO;2.

Wild, O., X. Zhu, and M. J. Prather (2000), Accurate simulation of in- and below cloud photolysis in tropospheric chemical models, *J. Atmos. Chem.*, *37*, 245–282.

Yashiro, H., S. Sugawara, K. Sudo, S. Akoi, and T. Nakazawa (2009), Temporal and spatial variations of carbon monoxide over the western part of the Pacific Ocean, *J. Geophys. Res.*, *114*, D08305, doi:10.1029/2008JD010876.

Zhang, Q., et al. (2009), Asian emissions in 2006 for the NASA INTEX-B mission, *Atmos. Chem. Phys.*, *9*, 5131–5153.